Supplementary material for

Climate variability shifts the vertical structure of phytoplankton in the Sargasso Sea

Johannes J. Viljoen[1,*], Xuerong Sun[1] and Robert J. W. Brewin[1].

[1]Centre for Geography and Environmental Science, Department of Earth and Environmental Science, Faculty of Environment, Science and Economy, University of Exeter, Cornwall, UK

*Corresponding author: j.j.viljoen@exeter.ac.uk

This supplementary material contains the following supplemental Figures, Tables and Text:

1 Supplemental Figures

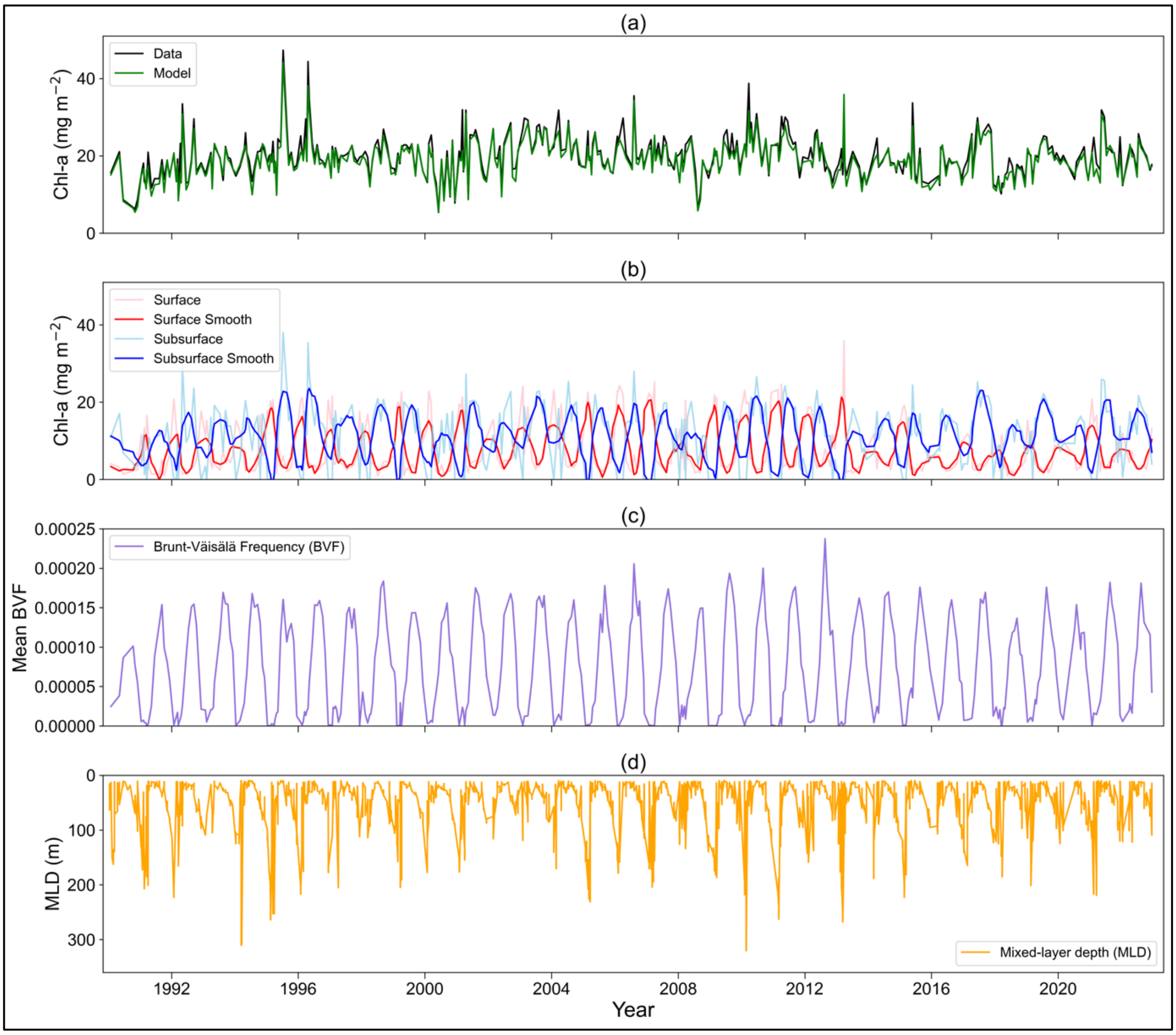

Figure S1 – Time series of column integrated Chl-a concentrations (mg m^{-2}), average Brunt-Väisälä buoyancy Frequency (BVF) and Mixed-layer depth (MLD). Depth-integration done from the surface to 1.5 times the euphotic depth (1.5 x Z_p; see Methods). (a) Integrated total Chl-a concentrations for the HPLC data and model output. (b) Integrated surface and subsurface Chl-a concentrations (smoothed data computed using Python *savgol_filter* with a window size of 11, polyorder of 2 and nearest mode). (c) Average BVF index of stratification in 1.5 times Z_p. (d) MLD from all CTD profiles included in the study (Max MLD of 321m in February 2010). See Figure S13b for Spearman relationship between integrated HPLC Chl-a data and modelled Chl-a.

Figure S2 – Time series of column integrated (1.5 x Z_p) POC and phytoplankton carbon concentrations (g m^{-2}), surface and subsurface phytoplankton carbon-to-chlorophyll ratios (C:Chl). (a) Integrated total POC concentrations for the data and model output. (b) Integrated phytoplankton carbon concentrations from model output. (c) Surface phytoplankton C:Chl ratios. (d) Subsurface phytoplankton C:Chl ratios. See Figure S13b for Spearman relationship between integrated POC data and integrated modelled POC.

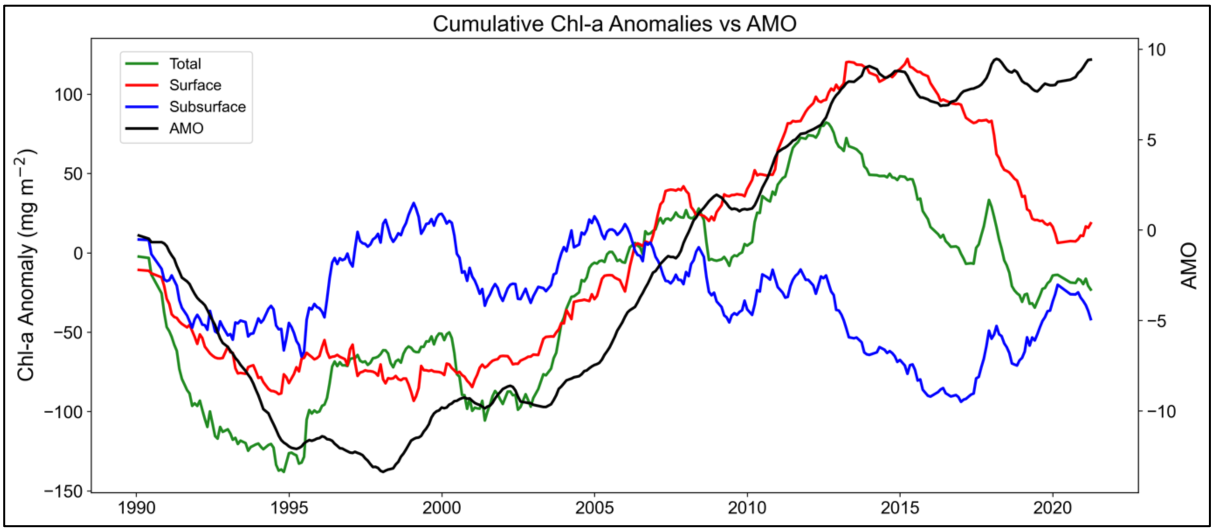

Figure S3 - Time series of cumulative Chl-a anomalies compared to the cumulative sum of the AMO index up until March-2021. Chl-a anomalies computed using mean climatology of the entire time series. This figure reflects the positive correlations of total and surface integrated Chl-a with the AMO index also shown in main text Figs. 2a and 2b where surface Chl-a trend had a stronger correlation compared to the total and subsurface showing no significant relationship with the AMO index.

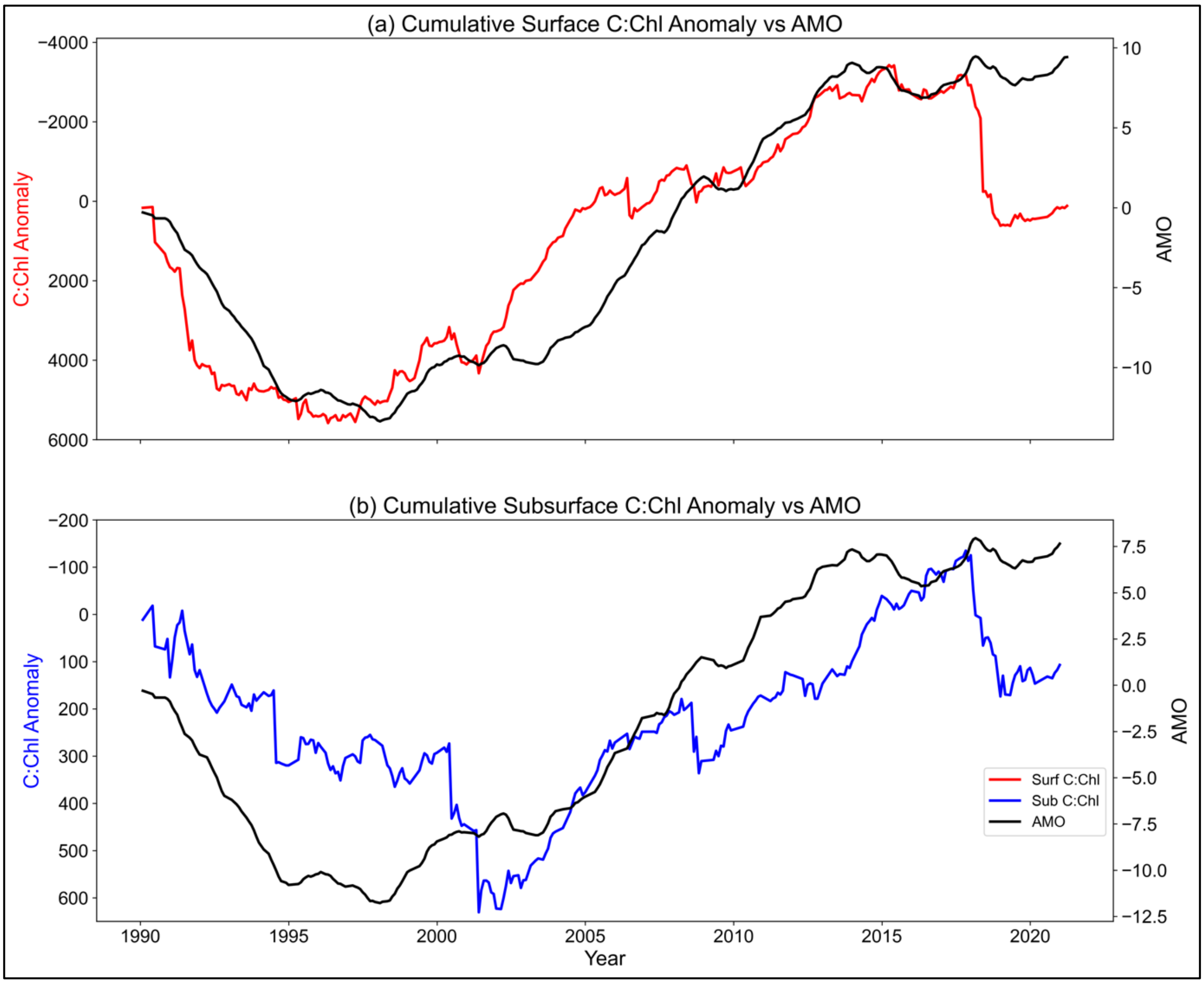

Figure S4 – Time series of cumulative sum of (a) surface and (b) subsurface C:Chla ratio anomalies (flipped y-axis) compared to the cumulative sum of the AMO index up until March-2021. C:Chl anomalies computed using the mean climatology of the entire time series. This figure reflects the negative correlations with the AMO index also shown in main text Figs. 2d and 2h where the surface C:Chl trends had a stronger negative correlation compared to the subsurface C:Chl trend.

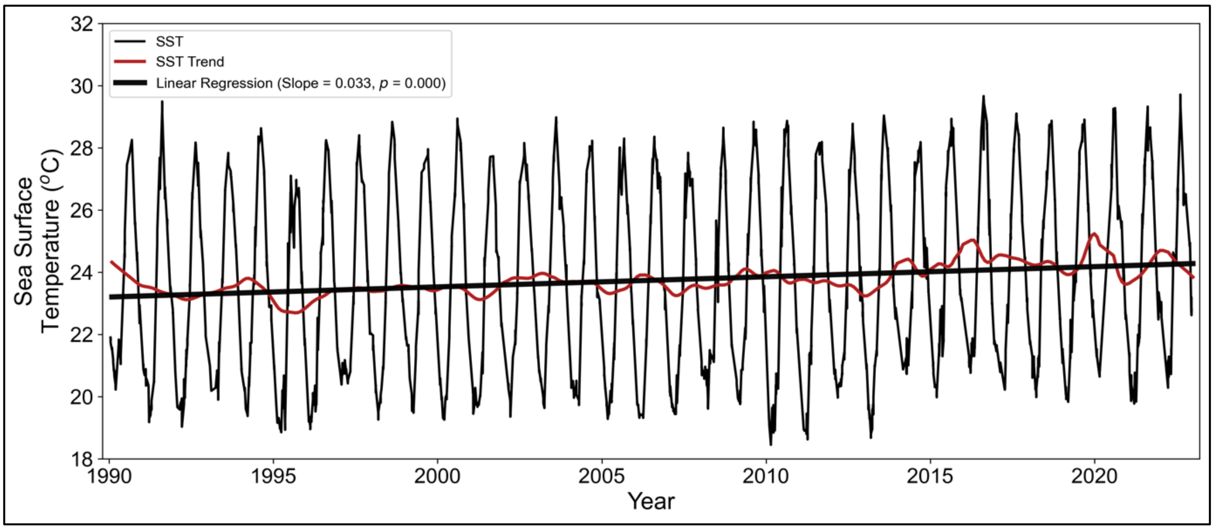

Figure S5 - Time series of surface ocean temperature (median upper in 11 m) used as sea surface temperature (SST). Thin black line: median CTD temperature in upper 11m for all BATS CTD profiles included in the study. Red line is the deseasonalised SST trend data. Thick black line is the linear regression applied to the SST trend. Deseasonalised trend extracted using the Python *MSTL* function with a period of 12 (see main text Methods).

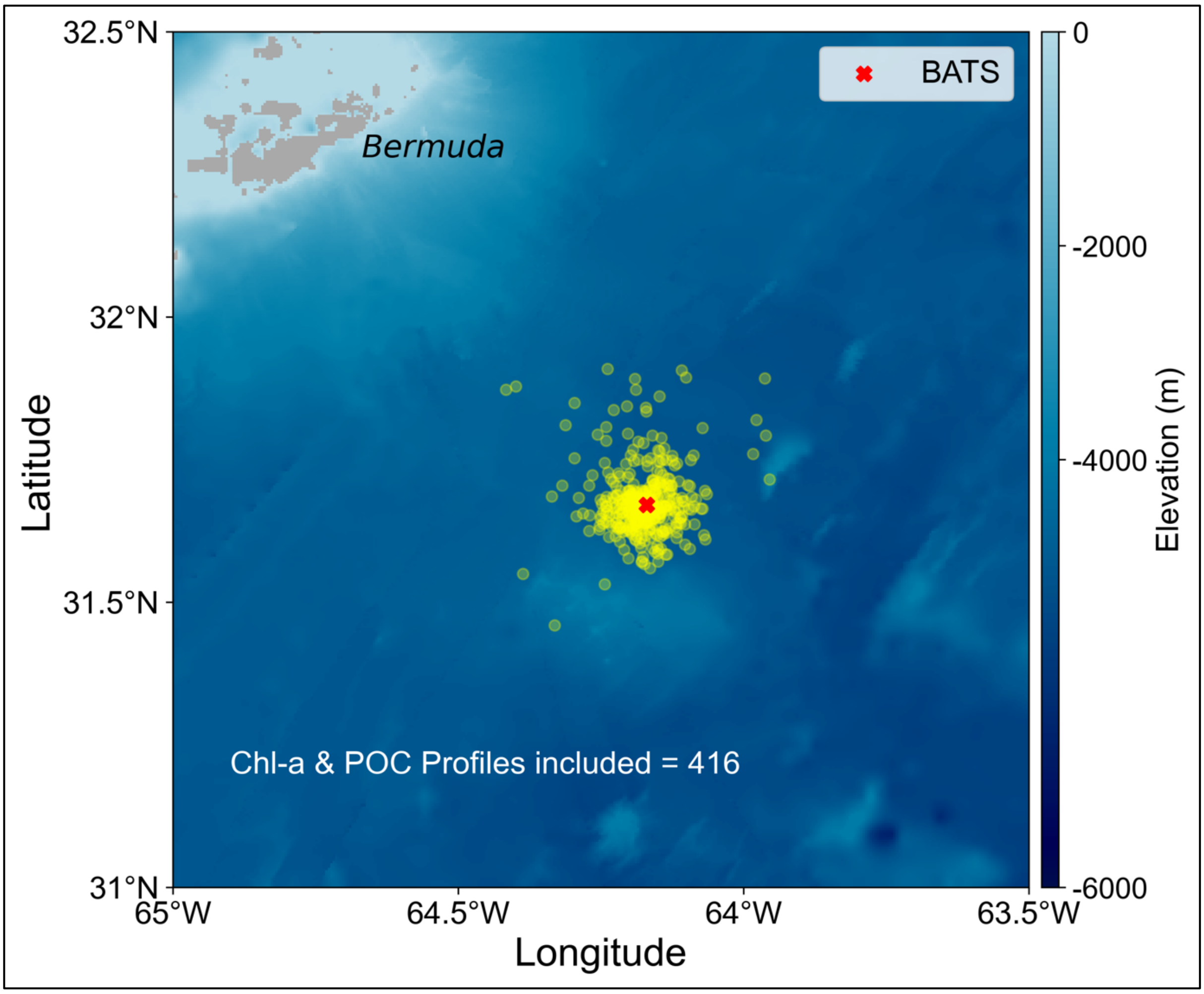

Figure S6 – Locations of bottle profiles from BATS included in this study (January 1990 to December 2022) in relation to the BATS site and Bermuda in the Sargasso Sea. The background bathymetry maps are from GEBCO 2021 (http://www.gebco.net/). Red cross is the current BATS location.

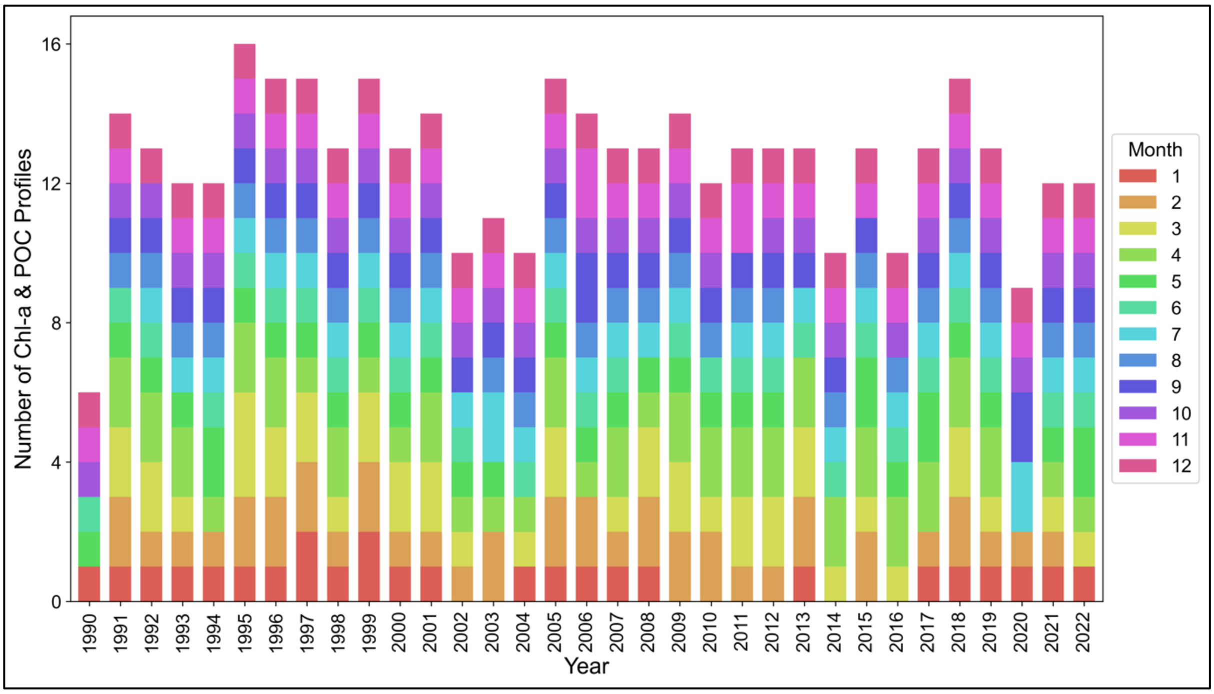

Figure S7 – Number of Chl-a and POC profiles per year coloured per month for from BATS used in this study (1990-2022).

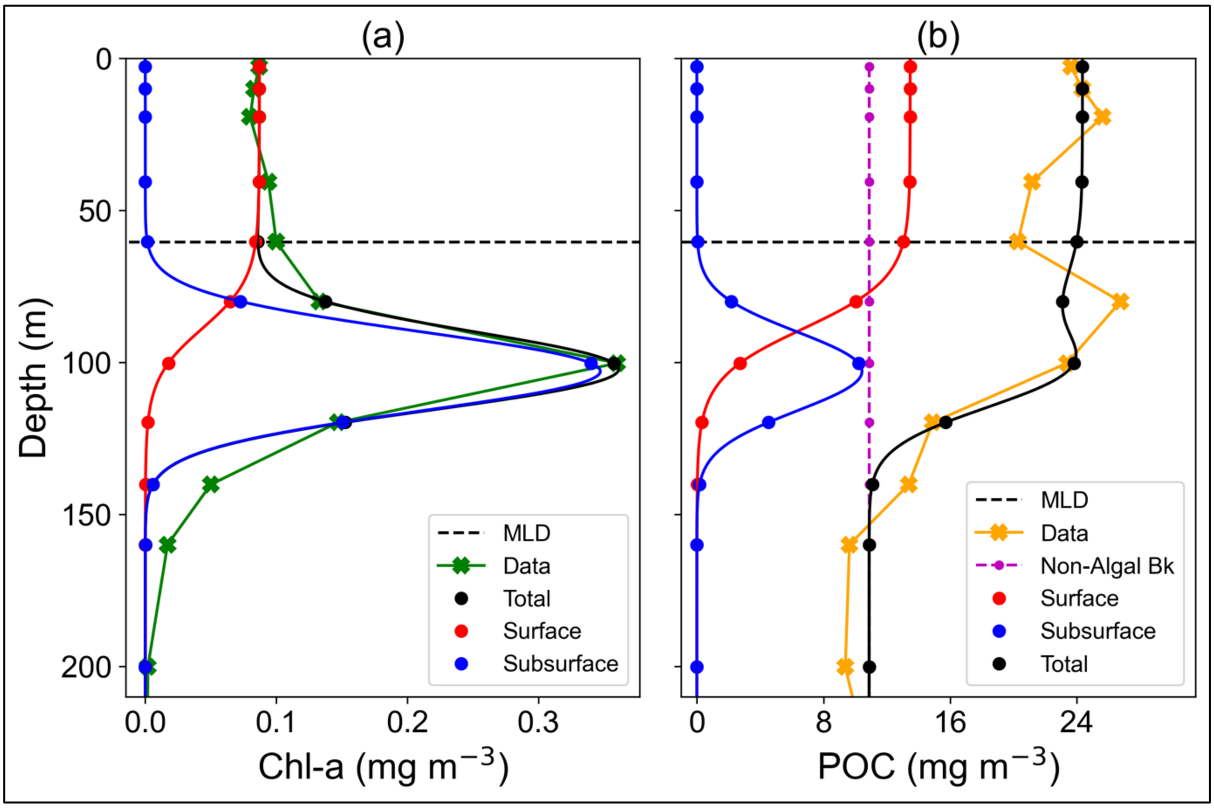

Figure S8 – Example of the modified Brewin et al. (2022) model applied to (a) HPLC Chl-a and (b) POC profiles from BATS (8-Dec-2004) in stratified conditions. The approach is designed to partition vertical profiles of Chl-a into two phytoplankton communities, a surface (Red) community that predominantly resides in the surface mixed-layer described using a Sigmoid function, and a subsurface (Blue) community living below the mixed-layer described using a Gaussian function. We extended the Brewin et al. (2022) model, for the first time, to coincident profiles of POC concentration by deriving a fixed carbon-to-chlorophyll ratio (C:Chl) per community for each profile, and assuming a fixed background carbon of non-algal particles (Non-algal Bk) for each profile. Thus, an estimate of phytoplankton carbon = surface carbon + subsurface carbon. See Code availability section in main text for Python code used to develop and fit the model.

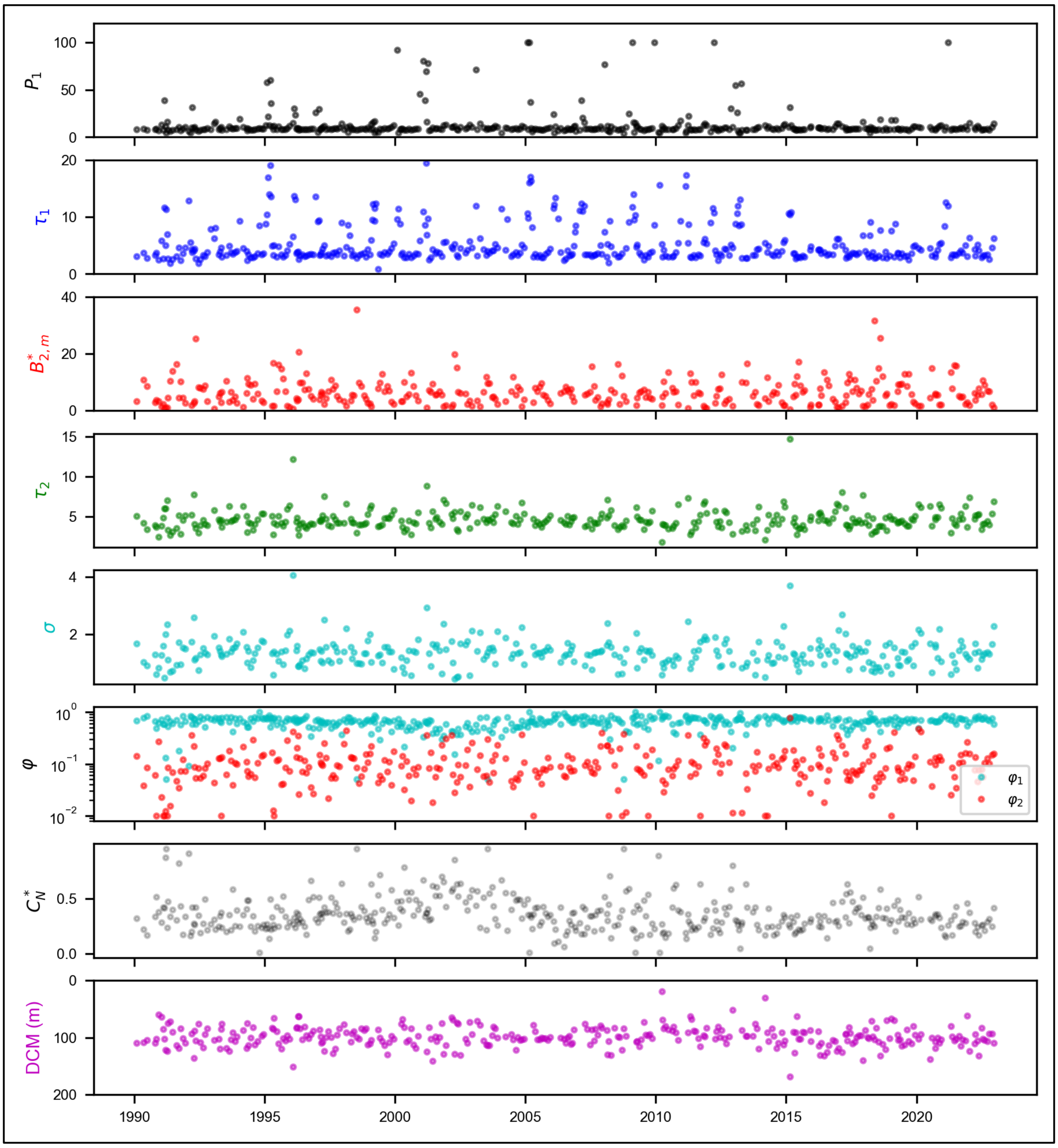

Figure S9 – Parameters of the model over BATS time-series derived from tuning the model to HPLC chlorophyll-a and POC. See main text methods for detailed model tuning and parameter descriptions. Modelled DCM depth computed from model parameter τ_2 divided by K_d for each profile.

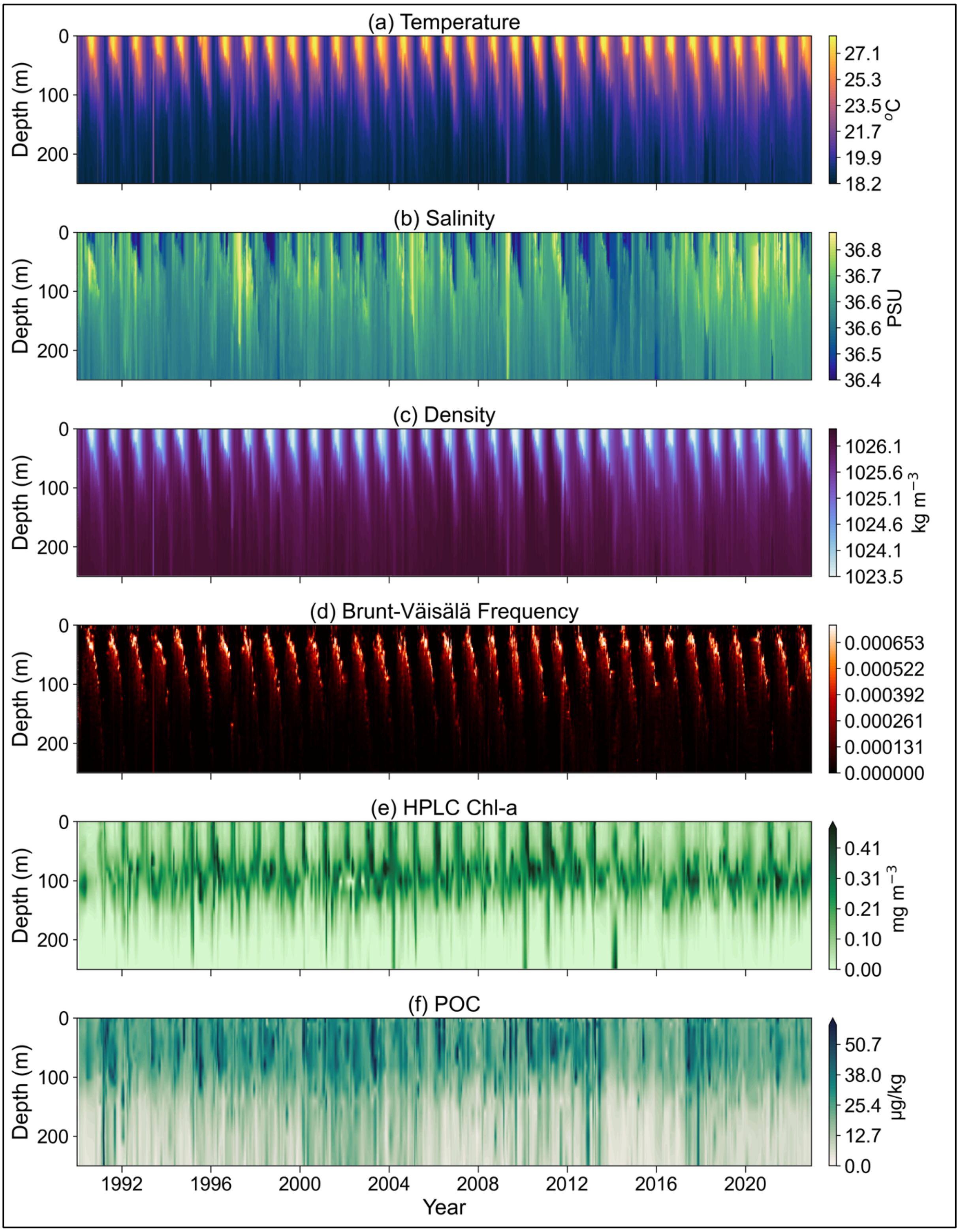

Figure S10 – Time series contour plots of BATS data used in this study in the upper 250 m of the water column. See main text for density and Brunt-Väisälä buoyancy Frequency (BVF) computation methods.

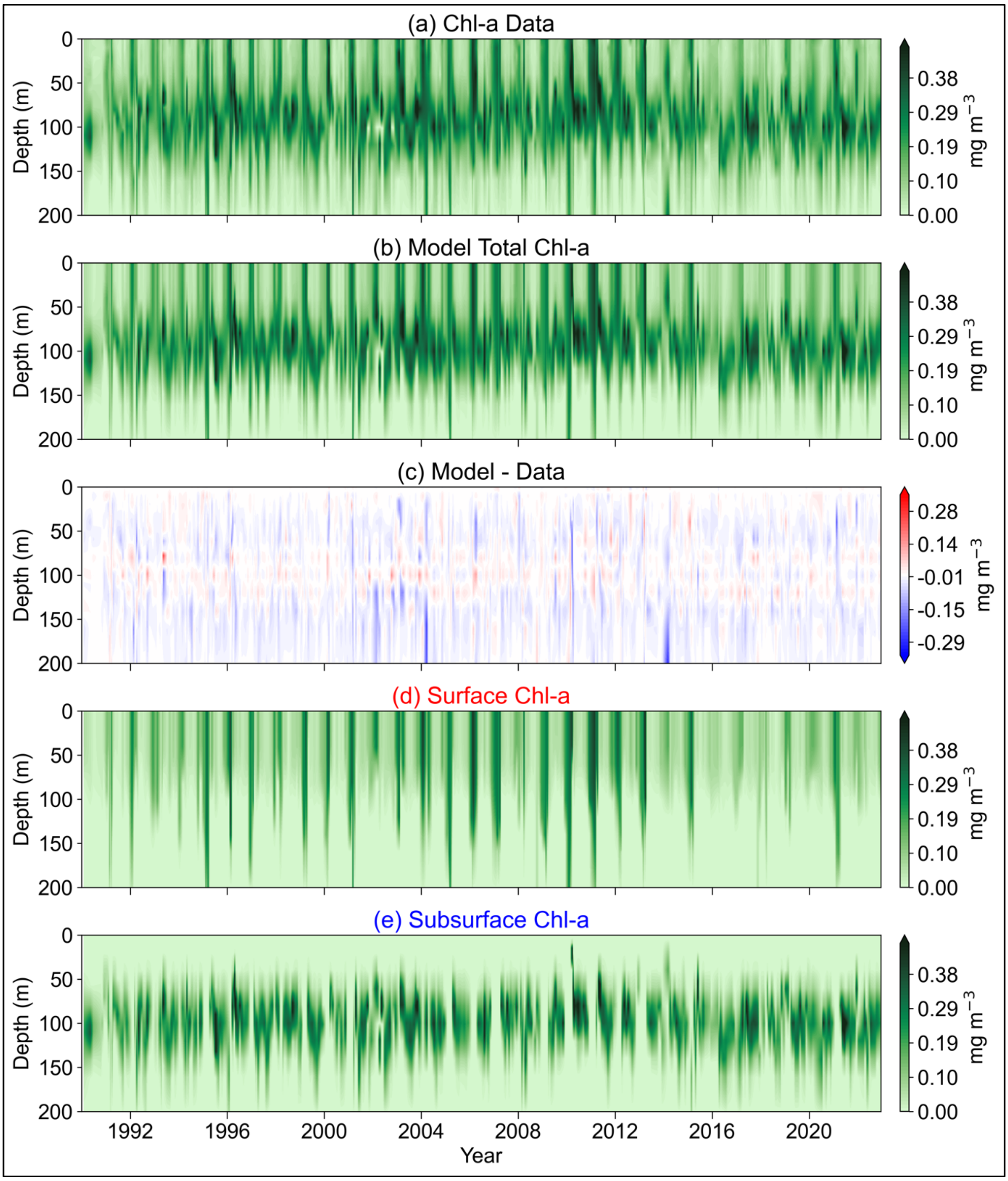

Figure S11 – Time series of Chl-a concentration (mg m^{-3}) model results in the top 250 m of the BATS site. (a) HPLC Chl-a concentration data from BATS. (b) Modelled total Chl-a from model tuning to data. (c) Differences in total Chl-a between model output and data. (d) Modelled Chl-a for surface phytoplankton. (e) Modelled Chl-a for subsurface phytoplankton.

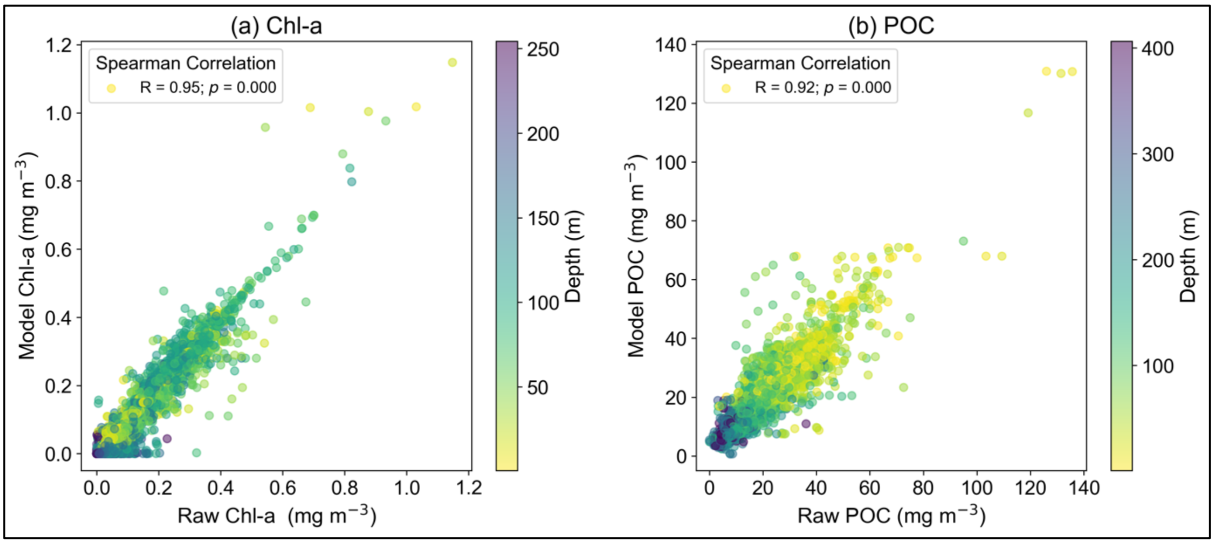

Figure S12 – Significant relationships between model results and raw data for (a) Chlorophyll-a concentration (Chl-a; mg m^{-3}) and (b) Particulate Organic Carbon concentration (POC; mg m^{-3}) over the entire BATS time series considered in this study.

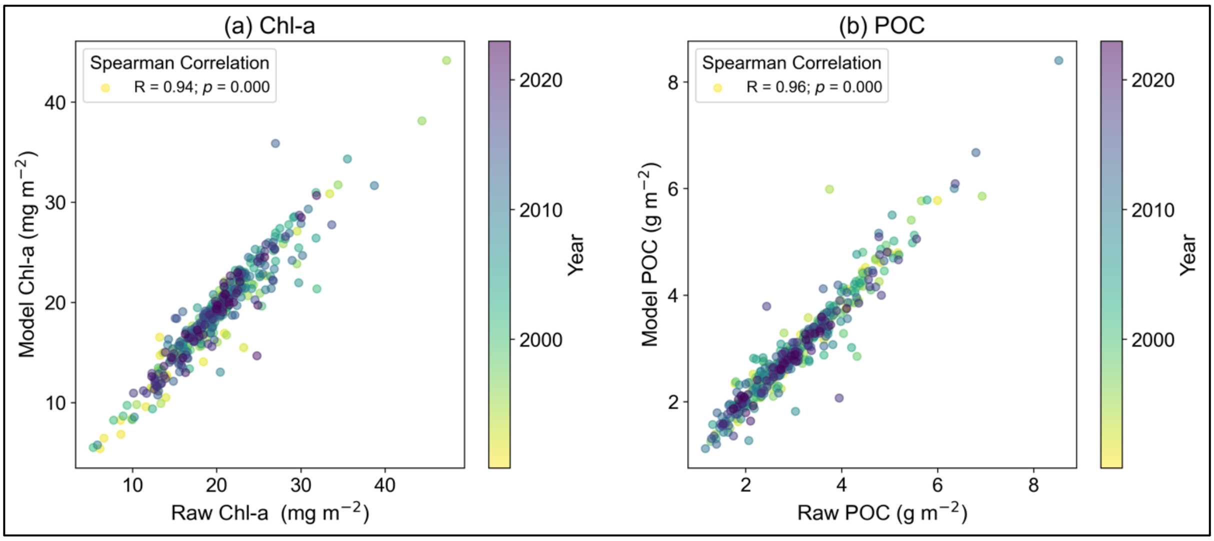

Figure S13 – Significant relationships between depth-integrated (1.5 x euphotic depth Z_p) model results and raw data for (a) Chlorophyll-a concentration (Chl-a; mg m^{-2}) and (b) Particulate Organic Carbon concentration (POC; g m^{-2}) over the entire BATS time series considered in this study.

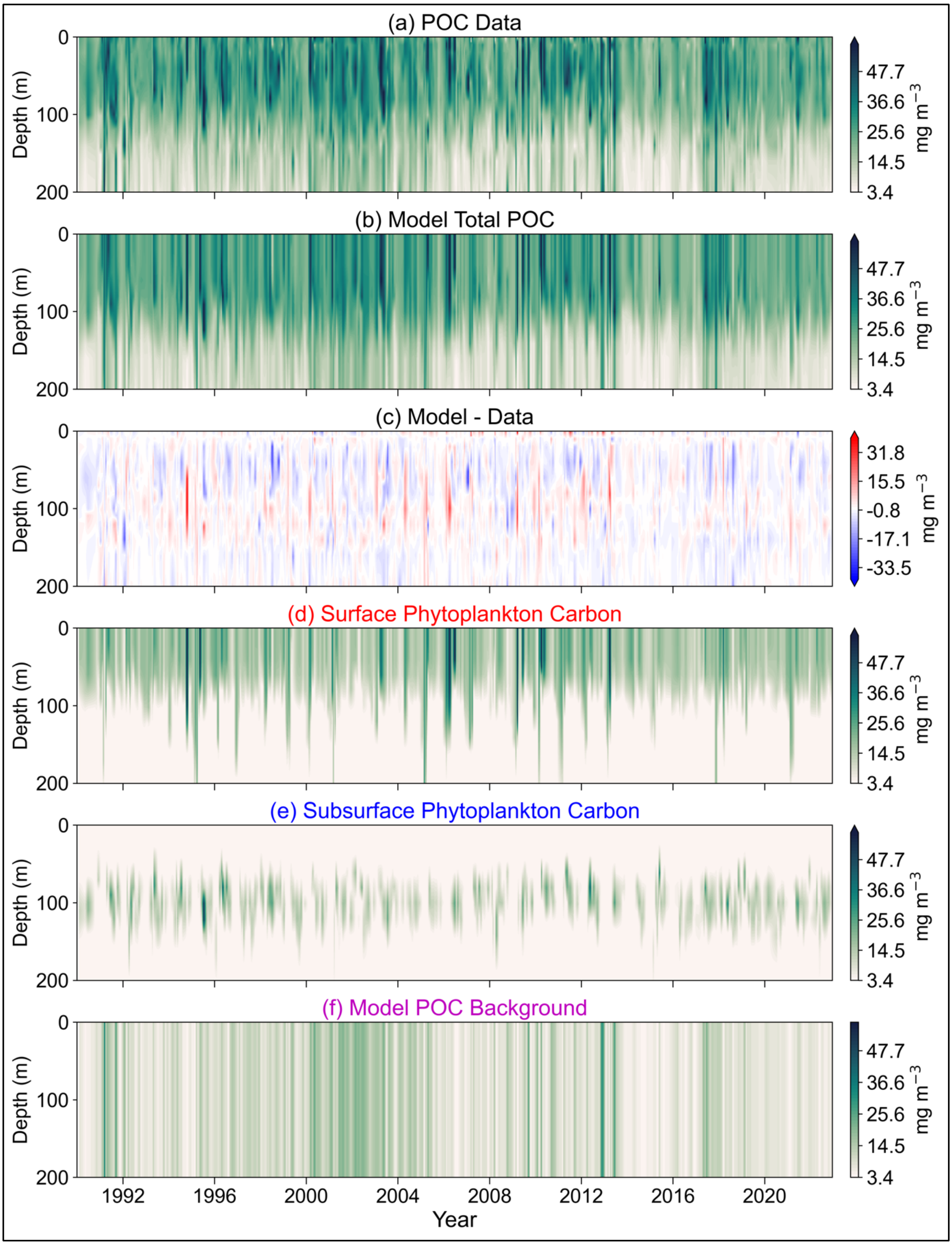

Figure S14 – Time series of POC concentration (mg m^{-3}) model results in the top 250 m of the BATS site. (a) POC concentration data from BATS. (b) Modelled total POC from model tuning to data. (c) Differences in total POC between model output and data. (d) Modelled surface phytoplankton carbon. (e) Modelled subsurface phytoplankton carbon. (f) Model POC background thought to be dominated by non-algal carbon.

2 Supplemental Tables

Table S1 – Summary statistics of various model results. POC - Integrated (1.5 x *Zp*) Particulate Organic Carbon; POC_{mod} – Integrated modelled POC; C – Integrated phytoplankton carbon; C:POC – median ratio of C to POC_{mod} in 1.5 x *Zp* (Figure S5); C:Chl – Carbon-to-chlorophyll ratio. MAD – Median Absolute Deviation calculated using Python function *median_abs_deviation* from *scipy.stats*.

	POC (g m^{-2})	POC_{mod} (g m^{-2})	C (g m^{-2})	C:POC	C:Chl surface	C:Chl subsurface
count	416	416	416	416	416	329
mean	3.08	2.99	1.82	0.64	289.4	44.8
MAD	0.67	0.57	0.38	0.09	136.1	11.5
std	1.06	1.00	0.74	0.16	256.3	28.1
min	1.16	1.12	0.1	0.05	6.0	1.2
25%	2.32	2.32	1.39	0.57	109.1	30.0
50%	2.94	2.85	1.76	0.67	228.6	41.4
75%	3.65	3.50	2.15	0.75	387.8	53.0
max	8.52	8.40	6.1	0.99	2328.1	226.1

Table S2 – Number of profiles per year for CTD, Chl-a and POC data from BATS included in this study (1990-2022). CTD – Conductivity Temperature Depth sensor; Chl-a – Chlorophyll-a, POC - Particulate Organic Carbon.

Year	CTD	Chl-a & POC
1990	51	6
1991	74	14
1992	102	13
1993	47	12
1994	82	12
1995	83	16
1996	88	15
1997	61	15
1998	61	13
1999	57	15
2000	55	13
2001	61	14
2002	45	10
2003	67	11
2004	88	10
2005	105	15
2006	141	14
2007	156	13
2008	154	13
2009	124	14
2010	137	12
2011	114	13
2012	128	13
2013	120	13
2014	102	10
2015	122	13
2016	123	10
2017	91	13
2018	106	15
2019	135	13
2020	75	9
2021	154	12
2022	113	12
Total	3222	416

Table S3 – Number of profiles per month for CTD, Chl-a and POC data from BATS included in this study (1990-2022). CTD – Conductivity Temperature Depth sensor; Chl-a – Chlorophyll-a, POC - Particulate Organic Carbon.

Month	CTD	Chl-a & POC
1	151	26
2	252	42
3	290	43
4	342	51
5	312	33
6	242	29
7	329	32
8	291	29
9	276	33
10	254	31
11	256	34
12	227	33
Total	3222	416

Table S4 – Number of profiles for each number of measurements per profile for Chl-a and POC data from BATS included in this study (1990-2022). Chl-a – Chlorophyll-a; POC - Particulate Organic Carbon.

Measurements per profile	Chl-a	POC
6	1	2
7	1	1
8	4	5
9	7	10
10	29	44
11	107	110
12	267	134
13		61
14		49
Total	416	416

3 Characteristics and patterns at BATS

The north-eastern Sargasso Sea hosts Bermuda Atlantic Time-series Study (BATS), an exceptional long-term study site with a water depth of 4680 m and situated south-east of Bermuda at 31°40'N 64° (Fig. S6). For more than three decades, various chemical, physical and biological variables have been regularly monitored on a monthly basis and biweekly in the spring (Jan-April) (Steinberg et al., 2001; Lomas et al., 2013). The sampling program included discrete bottle sampling via Conductivity Temperature Depth (CTD) rosette casts to analyse phytoplankton pigments using High Performance Liquid Chromatography (HPLC) and analyse POC. Being situated at the western boundary of the North Atlantic gyre, the Sargasso Sea is isolated from other ocean basins and terrestrial nutrient input. Hence, the epipelagic Sargasso Sea and BATS site can be characterised as oligotrophic (i.e., nutrient limited) with a deep euphotic zone (~100 m) (Lomas et al., 2013). Consequently, phytoplankton growth at BATS relies on deep mixing events such as seasonal winter entrainment, for nutrient replenishment. Accordingly, any changes in mixed-layer dynamics, such as increased stratification and decreased winter mixed-layer depth (MLD), have a detrimental impact on phytoplankton growth (D'Alelio et al., 2020; Lomas et al., 2022).

Physical and biological factors, namely temperature and Chl-a concentrations, demonstrate a distinct seasonal pattern over the 33-year BATS time series dataset considered here (Fig. S10). This is consistent with previous studies in the Sargasso Sea (Michaels et al., 1994; Lomas et al., 2013; Cotti-Rausch et al., 2016). Throughout the summer period, elevated temperatures, reduced salinity and less dense waters were observed, along with shallow MLDs and Chl-a vertical profiles characterized by a DCM. During summer, the water column also undergoes strong stratification, demonstrated by a higher Brunt-Väisälä buoyancy Frequency (BVF). In contrast, winter is characterised by lower temperatures, higher salinities, deep vertical mixing and more uniform distributions of Chl-a and POC concentrations.

4 Model Validation

4.1 Chlorophyll Model results

The modelled total Chl-a concentrations captured the seasonal patterns and dynamics of the HPLC Chl-a data over the entire 33-year BATS time series (Figs. S11a and b). The HPLC Chl-a measurements and the modelled total Chl-a concentrations were highly correlated ($R = 0.96$, $P < 0.001$; Fig. S12a). In some cases, where the profile showed complex dynamics with higher values at depth, the model underestimated Chl-a (Fig. S11c). Nonetheless, the model captured the higher and more uniform Chl-a during winter months, and a DCM during summer months, observed in the dataset. The model results showed that, in general, during winter the surface community dominates (up to 1.02 mg m^{-3} Chl-a), and the subsurface community, below the mixed-layer, is absent. During summer, with the presence of shallow mixed-layers, the subsurface community dominates the profiles (up to 0.95 mg m^{-3} Chl-a and sits usually between 87 m to 108 m depth) with a smaller contribution from the surface community (Figs. S11d and e). These seasonal variations are reflected through changes in the shape of the Chl-a profile and changes in model parameters over the time series (Fig. S10). Integrated concentrations (down to 1.5 times the Z_p, see methods) show that the total modelled Chl-a is in very good agreement with the Chl-a data over the time series ($R = 0.94$, $P < 0.001$; Figs. S1a, S13a).

4.2 POC Model Results

The extension of the model to POC measurements at BATS captured seasonal variations well (Figs. S14a–b). The data and modelled POC were strongly correlated ($R = 0.91$, $P < 0.001$; Fig. S12b). Furthermore, depth-integrated concentrations also reveal that the modelled POC is in good agreement with data over the time series (Fig. S2a) as shown by a strong significant correlation ($R = 0.95$, $P < 0.001$; Fig. S13b). The general patterns in the modelled surface and subsurface phytoplankton carbon concentrations (Figs. S14d-e) are similar to the Chl-a model (Figs. S11d-e). However, in contrast to the Chl-a time series, the POC time series showed a decreased prominence of deep maximums and higher concentrations within the surface (< 100m) in both the modelled and data contour plots (Figs. S14a-b). This observation is supported by the higher contribution of the surface community to POC over the time series compared to the subsurface community (Figs. S14d-e). The higher contribution to total POC of the surface community compared the subsurface community can be linked to the differences in the C:Chl ratio between the two communities which varied over the time series (Figs. S2c-d).

4.3 Modelled Phytoplankton Carbon

Owing to the difficulty in measuring phytoplankton carbon in the field (Lü et al., 2009; Maniaci et al., 2022), some phytoplankton carbon estimates are based on a constant contribution of phytoplankton carbon (C in this study) to total POC in the surface (e.g., Kostadinov et al., 2016). The estimation of phytoplankton biomass from Chl-a relies on the accurate estimation of a C:Chl ratio (Arteaga et al., 2016). Here our extension of the Brewin et al. (2022) model to discrete POC measurements allowed modelled estimates of phytoplankton

C:Chl not only for every profile but also separately for surface and subsurface. Integrated phytoplankton carbon (*C*) in this study (Fig. S2b) averaged at 1.82 ± 0.74 g m^{-2} (Table S1) and appears to be in agreement with recent flow-cytometry-based phytoplankton carbon estimates from BATS (Lomas et al., 2022). From the model results, the proportion of phytoplankton carbon to total POC, median carbon-to-POC ratio (*C:*POC), which averaged 0.64 ± 0.16 over the time series (Table S1), was notably higher than the recent flow cytometry estimated *C*:POC ratio average at BATS (0.30 ± 0.11; Lomas et al., 2022). Global satellite-based studies report proportions of *C* to POC to be higher (0.3-0.7) in less productive oligotrophic oceans such as the Sargasso Sea because of lower top-down grazing activity (Arteaga et al., 2016). This may suggest that the model overestimates the phytoplankton portion of total POC, possibly related to 1) an underestimation of non-algal POC due to the low number POC profiles, coincident with HPLC Chl-a profiles, that had measurements below 250m; or 2) our assumption in the model of no depth dependant variation in non-algal POC (see Methods). Nonetheless, our POC model provides an alternative approach to the estimation of phytoplankton carbon biomass, that captures depth-dependent variations in C:Chl ratios (Arteaga et al., 2016; Brewin et al., 2022).

5 References

Arteaga, L., Pahlow, M., and Oschlies, A. (2016). Modeled Chl:C ratio and derived estimates of phytoplankton carbon biomass and its contribution to total particulate organic carbon in the global surface ocean. *Global Biogeochem Cycles* 30, 1791–1810. doi: 10.1002/2016GB005458.

Brewin, R. J. W., Dall'Olmo, G., Gittings, J., Sun, X., Lange, P. K., Raitsos, D. E., Bouman, H. A., Hoteit, I., Aiken, J., and Sathyendranath, S. (2022). A Conceptual Approach to Partitioning a Vertical Profile of Phytoplankton Biomass Into Contributions From Two Communities. *J Geophys Res Oceans* 127, e2021JC018195. doi: 10.1029/2021JC018195.

Cotti-Rausch, B. E., Lomas, M. W., Lachenmyer, E. M., Goldman, E. A., Bell, D. W., Goldberg, S. R., and Richardson, T. L. (2016). Mesoscale and sub-mesoscale variability in phytoplankton community composition in the Sargasso Sea. *Deep Sea Research Part I: Oceanographic Research Papers* 110, 106–122. doi: 10.1016/J.DSR.2015.11.008.

D'Alelio, D., Rampone, S., Cusano, L. M., Morfino, V., Russo, L., Sanseverino, N., Cloern, J. E., and Lomas, M. W. (2020). Machine learning identifies a strong association between warming and reduced primary productivity in an oligotrophic ocean gyre. *Scientific Reports 2020 10:1* 10, 1–12. doi: 10.1038/s41598-020-59989-y.

Jackson, T., Sathyendranath, S., and Platt, T. (2017). An exact solution for modeling photoacclimation of the carbon-to-chlorophyll ratio in phytoplankton. *Front Mar Sci* 4, 283. doi: 10.3389/FMARS.2017.00283/BIBTEX.

Kostadinov, T. S., Milutinovi, S., Marinov, I., and Cabré, A. (2016). Carbon-based phytoplankton size classes retrieved via ocean color estimates of the particle size distribution. *Ocean Science* 12, 561–575. doi: 10.5194/OS-12-561-2016.

Lomas, M. W., Bates, N. R., Johnson, R. J., Knap, A. H., Steinberg, D. K., and Carlson, C. A. (2013). Two decades and counting: 24-years of sustained open ocean biogeochemical measurements in the Sargasso Sea. *Deep Sea Research Part II: Topical Studies in Oceanography* 93, 16–32. doi: 10.1016/J.DSR2.2013.01.008.

Lomas, M. W., Bates, N. R., Johnson, R. J., Steinberg, D. K., and Tanioka, T. (2022). Adaptive carbon export response to warming in the Sargasso Sea. *Nature Communications 2022 13:1* 13, 1–10. doi: 10.1038/s41467-022-28842-3.

Lü, S., Wang, X., and Han, B. (2009). A field study on the conversion ratio of phytoplankton biomass carbon to chlorophyll-a in Jiaozhou Bay, China. *Chinese Journal of Oceanology and Limnology* 27, 793–805. doi: 10.1007/s00343-009-9221-0.

Maniaci, G., Brewin, R. J. W., and Sathyendranath, S. (2022). Concentration and distribution of phytoplankton nitrogen and carbon in the Northwest Atlantic and Indian Ocean: A simple model with applications in satellite remote sensing. *Front Mar Sci* 0, 2152. doi: 10.3389/FMARS.2022.1035399.

Michaels, A. F., Knap, A. H., Dow, R. L., Gundersen, K., Johnson, R. J., Sorensen, J., Close, A., Knauer, G. A., Lohrenz, S. E., Asper, V. A., Tuel, M., and Bidigare, R. (1994). Seasonal patterns of ocean biogeochemistry at the U.S. JGOFS Bermuda Atlantic time-series study site. *Deep Sea Research Part I: Oceanographic Research Papers* 41, 1013–1038. doi: 10.1016/0967-0637(94)90016-7.

Roy, S., Sathyendranath, S., and Platt, T. (2017). Size-partitioned phytoplankton carbon and carbon-to-chlorophyll ratio from ocean colour by an absorption-based bio-optical algorithm. *Remote Sens Environ* 194, 177–189. doi: 10.1016/J.RSE.2017.02.015.

Sathyendranath, S., Platt, T., Kovač, Ž., Dingle, J., Jackson, T., Brewin, R. J. W., Franks, P., Marañón, E., Kulk, G., and Bouman, H. A. (2020). Reconciling models of primary production and photoacclimation [Invited]. *Applied Optics, Vol. 59, Issue 10, pp. C100-C114* 59, C100–C114. doi: 10.1364/AO.386252.

Steinberg, D. K., Carlson, C. A., Bates, N. R., Johnson, R. J., Michaels, A. F., and Knap, A. H. (2001). Overview of the US JGOFS Bermuda Atlantic Time-series Study (BATS): a decade-scale look at ocean biology and biogeochemistry. *Deep Sea Research Part II: Topical Studies in Oceanography* 48, 1405–1447. doi: 10.1016/S0967-0645(00)00148-X.